Excimer laser liftoff of AlGaN/GaN HEMTs on thick AlN heat spreaders

Cite as: Appl. Phys. Lett. 119, 132106 (2021); https://doi.org/10.1063/5.0064716
Submitted: 26 July 2021 • Accepted: 13 September 2021 • Published Online: 30 September 2021

🗓 Md Didarul Alam, Mikhail Gaevski, 🕩 Mohi Uddin Jewel, et al.







ARTICLES YOU MAY BE INTERESTED IN

Fabrication and analysis of InAIN/GaN metal-insulator-semiconductor high-electron-mobility transistors based on AIN/GaN superlattice channel

Applied Physics Letters 119, 143503 (2021); https://doi.org/10.1063/5.0064935

Degradation mechanism of Schottky P-GaN gate stack in GaN power devices under neutron irradiation

Applied Physics Letters 119, 133503 (2021); https://doi.org/10.1063/5.0065046

Growth of highly relaxed InGaN pseudo-substrates over full 2-in. wafers Applied Physics Letters 119, 131106 (2021); https://doi.org/10.1063/5.0064755

何QBLOX



Shorten Setup Time Auto-Calibration More Qubits

Fully-integrated
Quantum Control Stacks
Ultrastable DC to 18.5 GHz
Synchronized <<1 ns
Ultralow noise



100s qubits

visit our website >



Excimer laser liftoff of AlGaN/GaN HEMTs on thick AlN heat spreaders

Cite as: Appl. Phys. Lett. **119**, 132106 (2021); doi: 10.1063/5.0064716 Submitted: 26 July 2021 · Accepted: 13 September 2021 · Published Online: 30 September 2021







Md Didarul Alam, ^{a)} (b) Mikhail Gaevski, Mohi Uddin Jewel, (b) Shahab Mollah, (b) Abdullah Mamun, Kamal Hussain, Richard Floyd, (b) Grigory Simin, MVS Chandrashekhar, and Asif Khan (b)

AFFILIATIONS

Department of Electrical Engineering, University of South Carolina, Columbia, South Carolina 29208, USA

a) Author to whom correspondence should be addressed: ma57@email.sc.edu

ABSTRACT

We report on 193 nm excimer laser-based liftoff (LLO) of $Al_{0.26}Ga_{0.74}N/GaN$ high electron mobility transistors (HEMTs) with thick (t > 10 μ m) AlN heat spreading buffer layers grown over sapphire substrates. The use of the thick AlN heat spreading layer resulted in thermal resistance (R_{th}) of 16 K mm/W for as-fabricated devices on sapphire, which is lower than the value of ~25–50 K mm/W for standard HEMT structures on sapphire without the heat-spreaders. Soldering the LLO devices onto a copper heat sink led to a further reduction of R_{th} to 8 K mm/W, a value comparable to published measurements on bulk SiC substrates. The reduction in R_{th} by LLO and bonding to copper led to significantly reduced self-heating and drain current droop. A drain current density as high as 0.9 A/mm was observed despite a marginal reduction of the carrier mobility (~1800 to ~1500 cm²/V s). This is the highest drain current density and mobility reported to-date for LLO AlGaN/GaN HEMTs.

Published under an exclusive license by AIP Publishing. https://doi.org/10.1063/5.0064716

AlGaN/GaN high electron mobility transistors (HEMTs) have come a long way since their initial demonstration in 1993 and are desired for a multitude of applications in high-frequency and high-temperature power electronics. Recently, AlGaN/GaN HEMTs penetrated the consumer electronics with first-order applications. However, the performance of the devices is currently limited by severe self-heating effects that significantly reduce their efficacy in demanding applications that require high current density operation. One strategy to reduce the self-heating effects of GaN-based HEMTs is to use high thermal conductivity SiC or bulk AlN substrates. However, the cost of these substrates is $\sim\!\!3$ to 10-times that of sapphire substrates. Hence, strategies to improve the thermal management of the devices are highly desired for the full realization of III-nitride based device's potential in power electronics.

One promising approach for better thermal management of HEMTs on sapphire substrates is the LLO and bonding to a substrate with higher thermal conductivity. This approach has been used for visible InGaN and ultraviolet (UV) AlGaN LEDs^{12–19} and HEMTs (Table I). ^{20–26} The laser lifted-off devices are typically mounted on an Si, AlN, or a metallic heat sink, such as copper, commonly used in power electronics. ^{27,28} This leads to further challenges in assuring bonding with low thermal impedance and preserving the structural integrity of the III-nitride epi-layers. If the thickness of the III-nitride

layer is small compared to the solder thickness of 10– $50 \, \mu m$, it may wrinkle, crack, and be damaged during the solder reflow. However, too thick an epilayer can also introduce more thermal resistance. Ultraviolet LEDs with typical epilayer thicknesses of 2– $3 \, \mu m$ when flip-chipped by LLO¹⁵ are also susceptible to cracking. Due to this damage, LLO HEMTs typically are not soldered directly to highly thermally conductive metallic heat sinks. $^{21-25}$

For effective soldering to copper heat sink, III-nitride epilayers $>10 \,\mu m$ thick are required. We recently demonstrated the growth of such thick ultra-wide bandgap (UWBG) AlN layers on sapphire substrates with a room temperature thermal conductivity $320\,\mathrm{W/m\text{-}K.}^{29,30}$ This is much higher than the measured thermal conductivity values for GaN. These thick AlN/sapphire templates, therefore, not only are a suitable high thermal conductivity platform for AlGaN/GaN HEMTs but can also provide protection during the soldering of lifted-off devices to copper heat sink. However, it is more difficult to release AlN than GaN from the sapphire substrate because of its hardness and higher melting temperature. 15 It also requires a high fluence short wavelength deep ultraviolet (DUV) $\lambda = 193 \, \text{nm}$ excimer laser. The hardness and the high laser fluence liftoff invariably lead to excessive layer cracking. Developing LLO techniques for AlN liftoff from sapphire substrates is also highly desired for UWBG $Al_xGa_{1-x}N$ (x > 0.6) HEMTs, which are always grown with AlN buffer

TABLE I. Comparison of reported AIGaN/GaN HEMT laser liftoff. AF denotes as-fabricated (before LLO). Values that were not directly reported in the literature were estimated from the provided electrical characterization.

Ref. laser	Bonding agent	Carrier substrate	Mobility (cm ² /V s)	$m^2/V s$)	Sheet resist	Sheet resistance (Ω/sq)	Sheet carrier concentration (cm^{-2})	centration (cm ⁻
λ (nm) buffer layer with thickness (μm)	(thermal conductivity, W/mK)	(thermal conductivity, W/mK) (thickness, mm)	AF	TT	AF	TTO	AF	OTT
This work 193	In-Pb solder	Copper ($\sim 386^{50}$)	$\sim 1800 \; (V_T = -8.5 \; V)$	~1500 (V=-95V)	~310 (TLM)	\sim 310 (TLM) \sim 375 (TLM)	$\sim\!1\times10^{13}$	${\sim}1\times10^{13}$
Wang et al.	None	Glass $(\sim 0.8^{50})$	\sim 1520 (Hall) \sim 55		~484 (Hall)	$\sim 484 (Hall) \sim 1.6 \times 10^4$	$\sim 8.5 \times 10^{12}$	${\sim}8.8\times10^{12}$
193 GaN (2)		$(\sim 1 \text{ est.})$	$(V_{\rm T} = -3.4 \text{ V})$	$(V_T = -3.2 \text{ V})$	$\sim 1.1 \times 10^{4}$		(Hall)	510
Das <i>et al.</i> 355 GaN (4.3)	glue	AIN (\sim 180 $^{-2}$) (\sim 0.4 est.)	$\sim 102 \; ({ m V_T} = -5 \; { m V})$	~ 86 (V _T = -5.2 V)	$\sim 5.1 \times 10^{\circ}$	$\sim 5.7 \times 10^{\circ}$	$\sim 1.2 \times 10^{rz}$	$\sim 1.2 \times 10^{12}$
Chan <i>et al.</i> ^{23,a} 248 GaN (2.5)	Silver paint (\sim 9.1 ⁵⁶)	Si $(\sim 150^{25})$ $(\sim 0.5 \text{ est.})$	$\sim \! 1000 \; (Hall)$	\sim 1000 est. (Hall)	\sim 670 est.	~670 est. Not reported	$\sim 9.3 \times 10^{12}$ (Hall)	Not reported
Ji <i>et al.</i> ²⁴ 355 GaN (2.6)	Au/In/Au direct bond	Si (\sim 150) (\sim 0.5 est.)	$\sim 145 \text{ (V}_{\mathrm{T}} = -3.5 \text{ V} \sim 96 \text{ (V}_{\mathrm{T}} = -4 \text{ V}) \sim 5.7 \times 10^{3} \sim 7.3 \times 10^{3}$	$\sim 96 \; (V_T = -4 \; V)$	$\sim 5.7 \times 10^3$	$\sim 7.3 \times 10^3$	$\sim 8 \times 10^{12}$	$\sim 9 \times 10^{12}$

No field effect mobility was able to be extracted due to unavailability of device dimensions

layers. Thus, many previously demonstrated LLO approaches (Table I) for AlGaN/GaN HEMTs are not applicable to emerging UWBG III-N devices. $^{34-36}$

In this paper, we demonstrate the LLO of AlGaN/GaN HEMTs that were fabricated with $>\!10\,\mu\mathrm{m}$ thick high-quality AlN buffer layers on sapphire substrates. The lifted off layers were then soldered to copper heat sink to improve their capability to operate at high drain currents without a thermal droop attributed to self-heating. We show that the thermal performance is improved substantially and is like that of devices on bulk SiC substrates, the current gold-standard in heat sinks.

The AlGaN/GaN heterostructures used in this study were grown on c-plane sapphire by metalorganic chemical vapor deposition (MOCVD). A 2 µm AlN seed layer was first grown followed by the selective area growth (SAG) of 14 μ m thick AlN in 1 × 1 mm² window openings in a SiO₂ masking layer. The SiO₂ mask was then etched off using HF, and the first 2 µm thick AlN seed layer was also etched down by inductively coupled plasma (ICP), leaving a template with fully disconnected 16 μ m thick 1 \times 1 mm² blocks of AlN on the sapphire substrate. HEMT epilayers were then grown on these SAG AlN template by MOCVD, with a 3 μm undoped GaN channel layer and a 30 nm delta doped Al_{0.26}Ga_{0.74}N layer with a 1 nm AlN spacer in between. Delta doping was done by sandwiching a 10 nm Si-doped Al_{0.26}Ga_{0.74}N layer between two undoped 10 nm Al_{0.26}Ga_{0.74}N layers. Delta doping separates the dopants from the AlGaN/GaN 2DEG interface enabling higher sheet carrier concentration (n_s) , while minimizing carrier-impurity scattering that provides enhanced carrier mobility at high n_s . These effects both lead to an overall lowering of the sheet resistance. The device source/drain Ohmic contact metal stack Ti/Al/ Ti/Au (150/700/300/500 Å) was e-beam evaporated and annealed for 30 s at 950 °C under N2. This was followed by the gate-stack Ni/Au (1000/2000 Å) metallization. Source to drain spacing was 6 μ m, with a gate length of $\sim 2 \mu m$.

For the LLO process, the epitaxial side of the processed sample was bonded to UV tape, and a 193 nm excimer laser fluence of $\sim \! 1 \, \text{J/cm}^2$ was used. This yielded HEMT devices with $16 \, \mu \text{m}$ thick AlN heat spreading layers. The lifted-off surface was etched with 1:1 dilute HCl and Cl₂/Ar ICP to remove the damaged AlN layer. The sample was then transferred to copper using thermocompression bonding. The In-Pb solder temperature [$\sim \! 175\,^{\circ}\text{C}$ (Ref. 39)] is low enough to be compatible with flexible electronics. This procedure is schematically represented in Fig. 1. The HEMTs before and after LLO are also shown in Fig. 1. The output and transfer characteristics of the HEMT before and after LLO were measured using a parameter analyzer, while the capacitance–voltage (C–V) measurements were done using an LCR meter. Micro-Raman measurements were done at 473 nm. Highresolution x-ray diffractometry (HRXRD) was done using a triple-axis diffractometer at a wavelength $\lambda = 0.154 \, \text{nm}$.

Figure 2(a) shows the micro-Raman spectra of the $Al_{0.26}Ga_{0.74}N/GaN$ HEMT before and after LLO. The E_2 (high) peaks are only sensitive to strain unlike the $A_1(LO)$ peaks, which are also sensitive to free carriers. $^{40.41}$ The E_2 (high) phonon linewidth of the GaN channel layer, a measure of the crystalline quality, remained the same (\sim 7 cm $^{-1}$) before and after LLO. 40 Both AlN and GaN E_2 (high) phonons show 2.8 cm $^{-1}$ red-shift after LLO, indicating strain relief in both the AlN buffer and GaN channel layers, consistent with spatial Raman maps (Fig. SI1). This red-shift corresponds to a relief of compressive

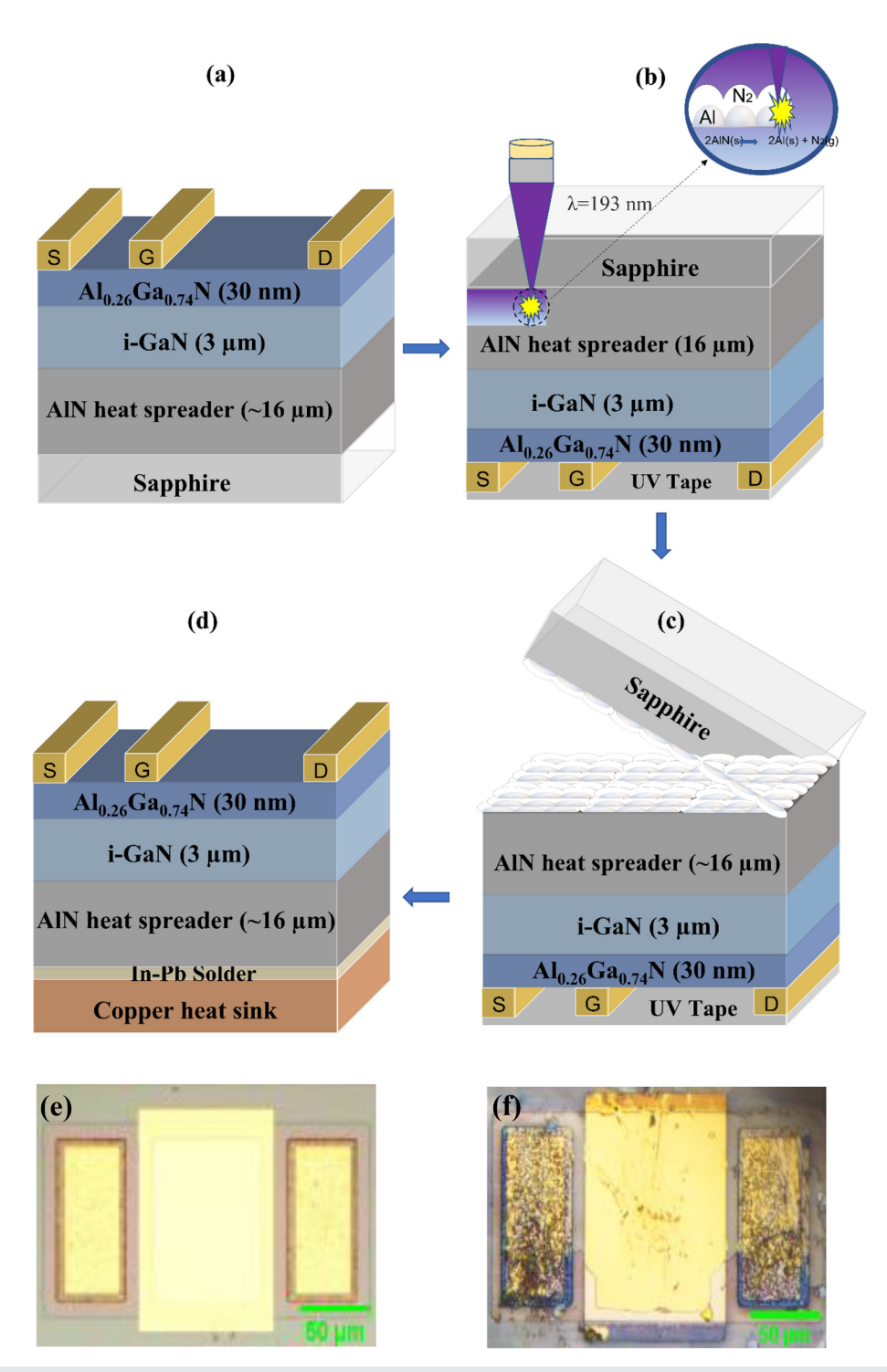
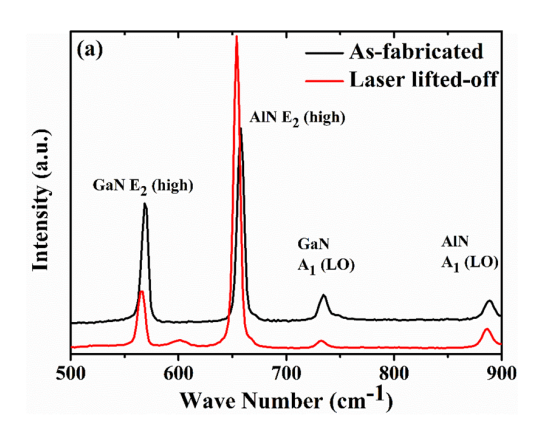


FIG. 1. LLO process flow of the $Al_{0.26}Ga_{0.74}N/GaN$ HEMT. (a) Device structure of the as-fabricated HEMT. (b) The HEMT structure was bonded to UV tape, and laser energy passes into the wafer acting on the AlN/sapphire interface dissociating AlN into Al(s) and $N_2(g)$. (c) After laser exposure, the sapphire substrate was separated. (d) The lifted-off AlN surface was cleaned and bonded to a copper heat sink using low melting temperature In-Pb solder. Optical images of the HEMT (e) before and (f) after LLO.



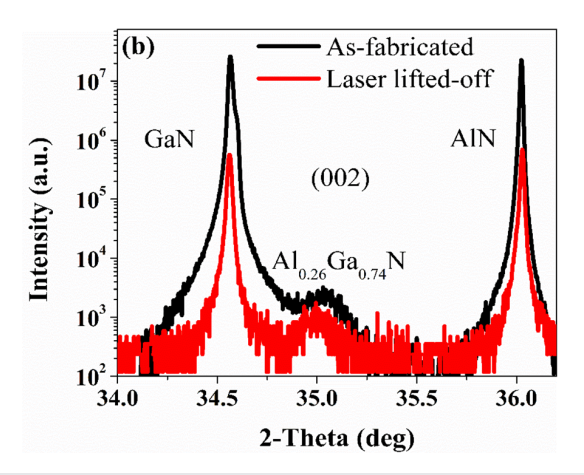


FIG. 2. (a) Raman spectra E_2 (high) and A_1 (LO) peaks of the HEMT before and after the LLO process. (b) HRXRD ω -2 θ coupled scan of 002 plane shows that the epitaxial registry of the AlGaN/GaN junction is preserved after LLO.

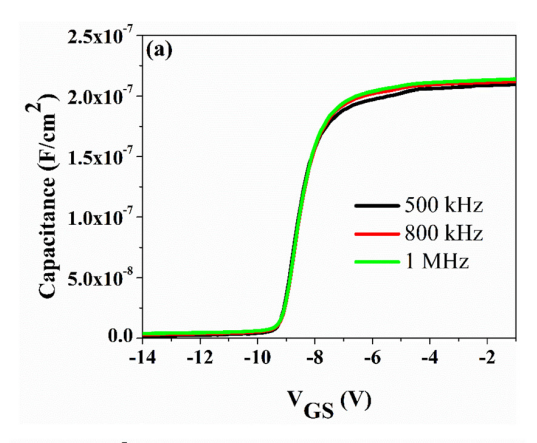
biaxial stress change –0.8 GPa calculated using a stress conversion coefficient –3.09 \pm 0.41 cm $^{-1}$ GPa $^{-1}$ $^{.42}$

This strain relaxation is supported by HRXRD [Fig. 2(b)] as demonstrated by the decrease in lattice constants from c=5.1879–5.1844 Å, while it increased from a=3.1813–3.1869 Å after LLO. Based on the lattice constants from HRXRD, biaxial strain $\varepsilon_a=1.6\times 10^{-3}$ was extracted corresponding to a stress relief of ~ 0.8 GPa (Fig. SI2), which is in excellent agreement with Raman. The relative biaxial strain of the barrier layer is preserved after LLO, as shown in Fig. 2(b) by HRXRD and by the n_s measured from frequency dependent C–V (Fig. 3). The n_s before and after LLO were calculated using the following equation was $\sim 1\times 10^{13}$ cm⁻², 36 indicating that the epitaxial registry of the AlGaN/GaN junction is preserved,

$$qn_s = \int_{V_T}^0 C_{G1}(V_{GS}) dV_{GS},\tag{1}$$

where q is the electron charge, V_T is the threshold voltage, C_{G1} is the gate capacitance per unit area , and V_{GS} is the gate-source voltage.

Figure 4 shows the output characteristics of the HEMT before and after LLO. The peak currents remained nearly the same as did



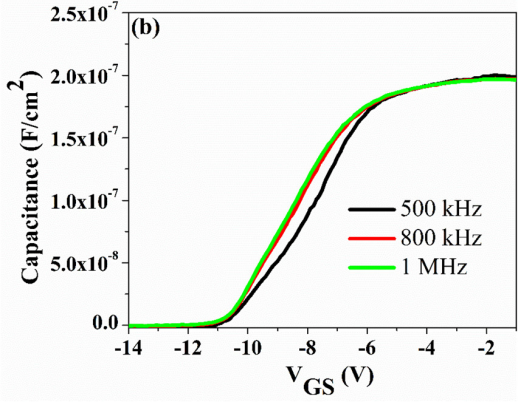


FIG. 3. Frequency dependent C-V characteristics of the Al_{0.26}Ga_{0.74}N/GaN HEMT (a) before and (b) after LLO.

 $R_C=0.66~\Omega$ mm before LLO to 0.73 Ω mm after LLO (Fig. SI3). This increase in R_C is most likely due to physical damage from transfer to and off the UV-tape [Fig. 1(f)], leading to peeling of the Ti/Au pad metals. Improved metal deposition at higher vacuum with a less adhesive transfer tape may reduce this damage, although post-transfer padformation could also solve this R_C increase. Before LLO, a reduction in drain current (I_{DS}) is observed in the saturation region with increasing drain voltage (V_{DS}) due to Joule heating, commonly known as self-heating, or thermal droop [Fig. 4(a)] that is significantly reduced in the LLO sample [Fig. 4(b)]. The distance from the heat source (HEMT channel) to the heat sink is now reduced from \sim 400 μ m of sapphire ($k \sim 34.6~W/mK$), down to \sim 16 μ m of AlN ($k \sim 320~W/mK$), eliminating a major source of R_{th} .

 R_{th} was measured using thermochromic paint that changes its color for a certain temperature under steady state electrical power. From Fig. 4(c), we calculated the R_{th} by 44

$$\Delta T = R_{th}P,\tag{2}$$

where ΔT is the channel temperature rise and P is the applied power. The as-fabricated devices on sapphire show R_{th} of $\sim 16 \,\mathrm{K}$ mm/W, which is lower than the typical $\sim 25-50 \,\mathrm{K}$ mm/W (Refs. 44–47) seen in GaN HEMTs grown directly on sapphire. This lower R_{th} is

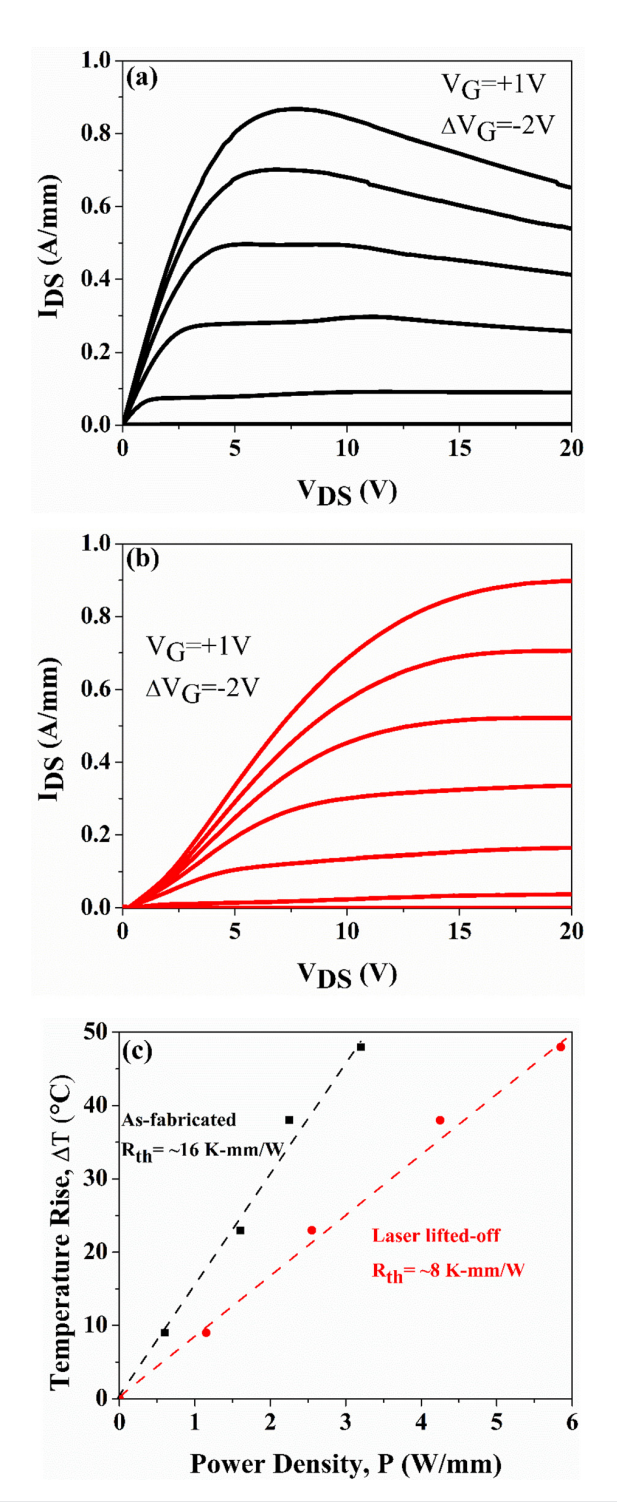


FIG. 4. Output characteristics of the $Al_{0.26}Ga_{0.74}N/GaN$ HEMT (a) before and (b) after LLO. (c) Channel temperature rise vs power dissipation comparison of the asfabricated and LLO structures.

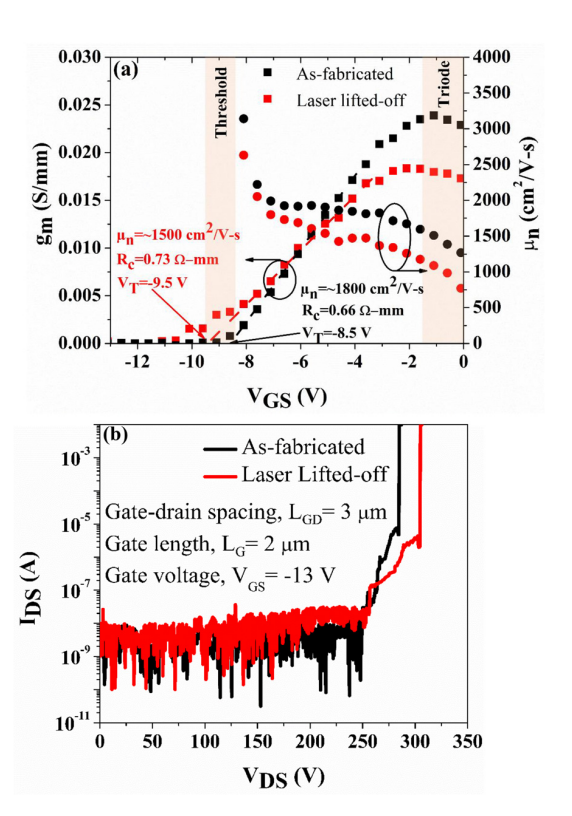


FIG. 5. (a) g_m and μ_n as a function of $V_{\rm GS}$ of the ${\rm Al}_{0.26}{\rm Ga}_{0.74}{\rm N/GaN}$ HEMT before and after LLO showing a marginal decrease in mobility after LLO. (b) Breakdown characteristics of the ${\rm Al}_{0.26}{\rm Ga}_{0.74}{\rm N/GaN}$ HEMT before and after LLO with gatedrain spacing, $L_{\rm GD}=3~\mu{\rm m}$.

attributed to the better heat spreading in the $\sim\!16\,\mu\mathrm{m}$ thick AlN due to its high intrinsic thermal conductivity. 29,30 AlN layers $<6\,\mu\mathrm{m}$ thick showed $\sim\!1/2$ the thermal conductivity compared to the thicker films, leading to less effective heat removal attributed to poorer AlN quality at the sapphire/AlN interface. 29 After LLO and soldering to the copper heat sink, R_{th} is $\sim\!8$ K mm/W, which is comparable to or less than the $\sim\!10\,\mathrm{K}$ mm/W for SiC substrates 45,46,48 using steady state techniques. The remaining R_{th} after sapphire removal and transfer onto copper heat sink is likely dominated by the poor thermal conductivity of In-Pb die-attach solder [$\sim\!41$ W/m K (Ref. 49)] compared to the excellent thermal conductivities of AlN [$\sim\!320\,\mathrm{W/m}\,\mathrm{K}$ (Refs. 29 and 30)] and copper [$\sim\!386\,\mathrm{W/m}\,\mathrm{K}$ (Ref. 50)].

The carrier mobility (μ_n) is extracted from the $I_{DS}-V_{GS}$ transfer curves (Fig. SI4) using 51

$$g_m = \frac{\partial I_{DS}}{\partial V_{GS}} = \mu_n C_{G1} \frac{W}{L} (V_{GS} - V_T), \tag{3}$$

where g_m is the transconductance, L is the gate-length, and W is the width. Figure 5(a) shows g_m vs V_{GS} , where x-intercept gives V_T , and it shifted negative by 1 V after LLO. From Fig. 5(a), the μ_n in 2D-channel is found to be $\sim 1800 \, \mathrm{cm}^2/\mathrm{V}$ s for the as-fabricated device, while it decreased to $\sim 1500 \, \mathrm{cm}^2/\mathrm{V}$ s after LLO. This μ_n is extracted at $V_{GS} = -5.1 \, \mathrm{V} \gg V_T$ to ensure the applicability of Eq. (3), while it is

much lower than the maximum $V_{GS} = +1 \, \mathrm{V}$ to minimize the influence of self-heating at high current levels. The lowered mobility is attributed to the dispersion seen in C–V, indicative of higher trap densities introduced by partial strain relaxation after LLO. ^{52–55} The μ_n is in excellent agreement with the sheet resistance from TLM (Table I), with the TLM sheet resistance $\sim 10\%$ lower than the transistor measurements.

Figure 5(b) shows the breakdown voltage characteristics of the Al_{0.26}Ga_{0.74}N/GaN HEMT before and after LLO with gate–drain spacing, $L_{GD}=3~\mu \mathrm{m}$. The breakdown voltages ($V_{BR,OFF}$) of the devices were measured at OFF-state conditions ($V_T\gg V_{GS}=-13~\mathrm{V}$) without junction edge termination. The results show $V_{BR,OFF}=\sim300~\mathrm{V}$, corresponding to breakdown field, $E_{BR,OFF}=\sim1~\mathrm{MV~cm^{-1}}$ for both asfabricated and LLO devices. Higher $V_{BR,OFF}$ may be achievable by proper junction edge termination, such as field plate extensions on the gate, along with optimized surface passivation. Nevertheless, the relative insensitivity of $V_{BR,OFF}$ to the LLO process underscores its viability in high voltage applications.

LLO of $Al_{0.26}Ga_{0.74}N/GaN$ HEMT with $>10~\mu m$ thick AlN templates from sapphire substrate was performed by a 193 nm ArF excimer laser and transferred onto a copper heat sink bonded by In-Pb solder. Incorporating a thick AlN heat spreading buffer layer instead of GaN led to a R_{th} of $\sim 16~K$ mm/W for as-fabricated devices on sapphire, which decreased further down to $\sim 8~K$ mm/W, comparable to published measurements on SiC substrates, after transferring the devices onto a copper heat sink. This is due to improved heat spreading in the thick AlN buffer with high intrinsic thermal conductivity and removal of large series R_{th} of the sapphire substrate. After LLO, the mobility decreased from ~ 1800 to $\sim 1500~cm^2/V$ s due to the introduction of traps during transfer. Drain current droop attributed to self-heating in as-fabricated HEMTs on sapphire is significantly reduced after transfer onto copper heat sink.

See the supplementary material for the Raman mapping images of both GaN E_2 (high) and AlN E_2 (high) mode in the access regions of both as-fabricated and LLO HEMT structures; lattice constants a and c of different epitaxial films as well as this sample before and after LLO determined by HRXRD measurements; room temperature Raman shifts vs corresponding residual stress change indicated by both E_2 (high) and A_1 (LO) modes; and TLM measurement results and transfer characteristics before and after LLO.

This research was supported by ARO under Contract No. W911NF-18-1-0029 monitored by Dr. M. Gerhold. The AlN template work was supported by ONR MURI program (Contract No. N00014-18-1-2429) monitored by Mr. Lynn Petersen. The characterization was partially supported by the National Science Foundation (NSF), ECCS Award Nos. 1711322, 1810116, and 1831954. We also acknowledge the UofSC ASPIRE program.

DATA AVAILABILITY

The data that support the findings of this study are available within the paper and its supplementary material.

REFERENCES

¹M. Asif Khan, X. Hu, A. Tarakji, G. Simin, J. Yang, R. Gaska, and M. S. Shur, Appl. Phys. Lett. 77, 1339 (2000).

- ²G. Simin, A. Tarakji, X. Hu, A. Koudymov, J. Yang, M. A. Khan, M. S. Shur, and R. Gaska, Phys. Status Solidi Appl. Res. 188, 219 (2001).
- ³V. Kumar, W. Lu, R. Schwindt, A. Kuliev, G. Simin, J. Yang, M. A. Khan, and I. Adesida, IEEE Electron Device Lett. 23, 455 (2002).
- ⁴U. K. Mishra, P. Parikh, and Y. F. Wu, Proc. IEEE **90**, 1022 (2002).
- ⁵X. Hu, J. Deng, N. Pala, R. Gaska, M. S. Shur, C. Q. Chen, J. Yang, G. Simin, M. A. Khan, J. C. Rojo, and L. J. Schowalter, Appl. Phys. Lett. 82, 1299 (2003).
- ⁶G. Simin, X. Hu, N. Ilinskaya, A. Kumar, A. Koudymov, J. Zhang, M. Asif Khan, R. Gaska, and M. S. Shur, Electron. Lett. 36, 2043 (2000).
- ⁷C. Lee, H. Wang, J. Yang, L. Witkowski, M. Muir, M. A. Khan, and P. Saunier, Electron. Lett. 38, 924 (2002).
- ⁸V. Kumar, W. Lu, F. A. Khan, R. Schwindt, A. Kuliev, G. Simin, J. Yang, M. Asif Khan, and I. Adesida, Electron. Lett. 38, 252 (2002).
- ⁹See https://www.infineon.com/cms/en/product/power/gan-hemt-galliumnitride-transistor/ for more information on applications of AlGaN/GaN HEMTs in consumer electronics (accessed 07 July 2021).
- ¹⁰See https://www.qorvo.com/products/discrete-transistors/gan-hemts for more information on applications of AlGaN/GaN HEMTs in consumer electronics (accessed 07 July 2021).
- ¹¹M. A. Fraga, M. Bosi, and M. Negri, Advanced Silicon Carbide Devices Process (InTech, 2015), Chap. 1.
- ¹²Y. Sun, S. Trieu, T. Yu, Z. Chen, S. Qi, P. Tian, J. Deng, X. Jin, and G. Zhang, Semicond. Sci. Technol. 26, 085008 (2011).
- ¹³S. Hwang, D. Morgan, A. Kesler, M. Lachab, B. Zhang, A. Heidari, H. Nazir, I. Ahmad, J. Dion, Q. Fareed, V. Adivarahan, M. Islam, and A. Khan, Appl. Phys. Express 4, 032102 (2011).
- ¹⁴ H. Aoshima, K. Takeda, K. Takehara, S. Ito, M. Mori, M. Iwaya, T. Takeuchi, S. Kamiyama, I. Akasaki, and H. Amano, Phys. Status Solidi 9, 753 (2012).
- ¹⁵M. Lachab, F. Asif, B. Zhang, I. Ahmad, A. Heidari, Q. Fareed, V. Adivarahan, and A. Khan, Solid State Electron. 89, 156 (2013).
- ¹⁶F. Asif, H. C. Chen, A. Coleman, M. Lachab, I. Ahmad, B. Zhang, Q. Fareed, V. Adivarahan, and A. Khan, Jpn. J. Appl. Phys., Part 1 52, 08JG14 (2013).
- ¹⁷H. K. Cho, O. Krüger, A. Külberg, J. Rass, U. Zeimer, T. Kolbe, A. Knauer, S. Einfeldt, M. Weyers, and M. Kneissl, Semicond. Sci. Technol. 32, 12LT01 (2017).
- ¹⁸S. Bornemann, N. Yulianto, H. Spende, Y. Herbani, J. D. Prades, H. S. Wasisto, and A. Waag, Adv. Eng. Mater. 22, 1901192 (2020).
- ¹⁹K. Kawasaki, C. Koike, Y. Aoyagi, and M. Takeuchi, Appl. Phys. Lett. 89, 261114 (2006).
- 20X. Wang, C.-F. Lo, L. Liu, C. V. Cuervo, R. Fan, S. J. Pearton, B. Gila, M. R. Johnson, L. Zhou, D. J. Smith, J. Kim, O. Laboutin, Y. Cao, and J. W. Johnson, J. Vac. Sci. Technol. B 30, 051209 (2012).
- ²¹J. Das, W. Ruythooren, R. Vandersmissen, J. Derluyn, M. Germain, and G. Borghs, Phys. Status Solidi 2, 2655 (2005).
- ²²K. K. Leung, C. P. Chan, W. K. Fong, M. Pilkuhn, H. Schweizer, and C. Surya, J. Cryst. Growth 298, 840 (2007).
- ²³C. P. Chan, K. K. Leung, M. Pilkuhn, C. Surya, T. M. Yue, G. Pang, and H. Schweizer, Phys. Status Solidi 204, 914 (2007).
- ²⁴H. Ji, J. Das, M. Germain, and M. Kuball, Solid State Electron. **53**, 526 (2009).
- 25 T. S. Kang, X. T. Wang, C. F. Lo, F. Ren, S. J. Pearton, O. Laboutin, Y. Cao, J. W. Johnson, and J. Kim, J. Vac. Sci. Technol. B 30, 011203 (2012).
- ²⁶F. Guo, Q. Wang, H. Xiao, L. Jiang, W. Li, C. Feng, X. Wang, and Z. Wang, Semicond. Sci. Technol. 35, 095024 (2020).
- ²⁷J. Schulz-Harder, Microelectron. Reliab. 43, 359–365 (2003).
- ²⁸S. Yin, K. J. Tseng, and J. Zhao, Appl. Therm. Eng. **52**, 120 (2013).
- ²⁹Z. Cheng, Y. R. Koh, A. Mamun, J. Shi, T. Bai, K. Huynh, L. Yates, Z. Liu, R. Li, E. Lee, M. E. Liao, Y. Wang, H. M. Yu, M. Kushimoto, T. Luo, M. S. Goorsky, P. E. Hopkins, H. Amano, A. Khan, and S. Graham, Phys. Rev. Mater. 4, 044602 (2020).
- ³⁰Y. R. Koh, Z. Cheng, A. Mamun, M. S. Bin Hoque, Z. Liu, T. Bai, K. Hussain, M. E. Liao, R. Li, J. T. Gaskins, A. Giri, J. Tomko, J. L. Braun, M. Gaevski, E. Lee, L. Yates, M. S. Goorsky, T. Luo, A. Khan, S. Graham, and P. E. Hopkins, ACS Appl. Mater. Interfaces 12, 29443 (2020).
- ³¹Q. Zheng, C. Li, A. Rai, J. H. Leach, D. A. Broido, and D. G. Cahill, Phys. Rev. Mater. 3, 014601 (2019).
- ³²H. Shibata, Y. Waseda, H. Ohta, K. Kiyomi, K. Shimoyama, K. Fujito, H. Nagaoka, Y. Kagamitani, R. Simura, and T. Fukuda, Mater. Trans. 48, 2782 (2007).

- ³³A. Jezowski, B. A. Danilchenko, M. Boćkowski, I. Grzegory, S. Krukowski, T. Suski, and T. Paszkiewicz, Solid State Commun. 128, 69 (2003).
- 34S. Mollah, K. Hussain, A. Mamun, M. Gaevski, G. Simin, M. V. S. Chandrashekhar, and A. Khan, Appl. Phys. Express 14, 014003 (2021).
- 35 M. Gaevski, S. Mollah, K. Hussain, J. Letton, A. Mamun, M. U. Jewel, M. Chandrashekhar, G. Simin, and A. Khan, Appl. Phys. Express 13, 094002 (2020).
- 36 H. Xue, K. Hussain, V. Talesara, T. Razzak, M. Gaevski, S. Mollah, S. Rajan, A. Khan, and W. Lu, Phys. Status Solidi 15, 2000576 (2021).
- 37S. A. Vitusevich, A. M. Kurakin, N. Klein, M. V. Petrychuk, A. V. Naumov, and A. E. Belyaev, IEEE Trans. Device Mater. Reliab. 8, 543 (2008). 38 Z. Y. Fan, J. Li, J. Y. Lin, and H. X. Jiang, Appl. Phys. Lett. 81, 4649 (2002).
- 39See https://www.indium.com/blog/indium-lead-inpb-solder-alloys-for-reliablegold-interconnects-in-semiconductor-assembly.php for more information on melting temperature of In-Pb solder; accessed 7 July 2021.
- 40 M. Kuball, Surf. Interface Anal. 31, 987 (2001).
- ⁴¹Y. Huang, X. D. Chen, S. Fung, C. D. Beling, and C. C. Ling, J. Phys. D: Appl. Phys. 37, 2814 (2004).
- 42S. Choi, E. Heller, D. Dorsey, R. Vetury, and S. Graham, J. Appl. Phys. 113, 093510 (2013).
- 43S. Chae, K. A. Mengle, R. Lu, A. Olvera, N. Sanders, J. Lee, P. F. P. Poudeu, J. T. Heron, and E. Kioupakis, Appl. Phys. Lett. 117, 102106 (2020).
- 44R. Gaska, A. Osinsky, J. W. Yang, and M. S. Shur, IEEE Electron Device Lett. 19, 89 (1998).
- 45 M. Kuball, J. W. Pomeroy, R. Simms, G. J. Riedel, H. Ji, A. Sarua, M. J. Uren, and T. Martin, in IEEE Compound Semiconductor Integrated Circuit Symposium, Technical Digest (IEEE, 2007), Vol. 116.

- ⁴⁶M. Kuball, J. M. Hayes, M. J. Uren, T. Martin, J. C. H. Birbeck, R. S. Balmer, and B. T. Hughes, <u>IEEE Electron Device Lett. 23</u>, 7 (2002).

 47 J. Sun, H. Fatima, A. Koudymov, A. Chitnis, X. Hu, H. M. Wang, J. Zhang,
- G. Simin, J. Yang, and M. A. Khan, IEEE Electron Device Lett. 24, 375
- 48 J. G. Felbinger, M. V. S. Chandra, Y. Sun, L. F. Eastman, J. Wasserbauer, F. Faili, D. Babic, D. Francis, and F. Ejeckam, IEEE Electron Device Lett. 28, 948 (2007).
- ⁴⁹See https://www.indium.com/applications/thermal-management/#thermal-kvalues-list for more information on thermal conductivity of In-Pb solder; accessed 7 July 2021.
- 50 See http://hyperphysics.phy-astr.gsu.edu/hbase/Tables/thrcn.html for more information on thermal conductivity of copper; accessed 7 July 2021.
- ⁵¹F. Roccaforte, G. Greco, P. Fiorenza, and F. Iucolano, Materials 12, 1599
- ⁵²M. Chu, A. D. Koehler, A. Gupta, S. Parthasarathy, M. O. Baykan, S. E. Thompson, and T. Nishida, Materials and Reliability HandbOok for Semiconductor Optical and Electron Devices (Springer, 2013), Vol. 381.
- 53B. Shankar, A. Soni, S. Raghavan, and M. Shrivastava, IEEE Trans. Device Mater. Reliab. 20, 767 (2020).
- ⁵⁴T. Beechem, A. Christensen, D. S. Green, and S. Graham, J. Appl. Phys. 106, 114509 (2009).
- 55 J. A. del Alamo and J. Joh, Microelectron. Reliab. 49, 1200 (2009).
- 56See https://www.tedpella.com/technote_html/16047-TN-V1-06232009.pdf for more information on thermal conductivity of silver paint; accessed 07 July